Remnant charge of slow multicharged ions scattered from a gold surface

R. D. Miller,* G. Wattuhewa,† R. H. Hughes, D. O. Pederson, and X. M. Ye‡
Department of Physics, University of Arkansas, Fayetteville, Arkansas 72701
(Received 9 December 1991)

A time-of-flight technique has been used to measure the remnant charge of laser-produced pulses of multicharged C^{k+} ($k=1-4$), Al^{m+} ($m=3-6$), and Pb^{n+} ($n=2-6$) ions incident on a clean amorphous Au surface under UHV conditions. Remnant charge states were investigated for 15°, 30°, and 45° scattering angles for C and Al ions and 15° only for Pb. For all angles considered, C and Pb were found to be completely neutralized after scattering from the Au surface. The remnant singly charged state of Al, however, was detected in all instances in addition to neutral Al atoms with charge fractions being ~60%. Detailed charge fractions were determined for incident Al^{z+} ($z=3-5$) with energies ≈400 eV/z. The scattering angle was fixed at 15° while the incoming angle was varied from 3° to 12°. The results obtained could be fitted with the expected form of a decaying exponential. The charge fractions showed a dependence on the outgoing path while being independent of the incoming path. Although the characteristic velocity for a particular incident Al^{z+} charge state (hence constant energy determined by an electrostatic analyzer) was found to be constant, the inclusive case for all three aluminum incident charge states required an energy-dependent characteristic velocity in order to obtain a reasonable fit for the remnant charge fraction as a function of a decaying exponential. The results are interpreted to be indicative of the importance of the ground-state energy level of the projectile as compared to the Fermi level of the metal and how it evolves close to the metal surface as well as the importance of the distance of closest approach of the projectile to the metal first atomic layer.

INTRODUCTION

The scattering of low-energy (less than a few keV) ions from surfaces has been attracting increasing attention in recent years as a very sensitive probe of the scattering surface. Low-energy ion scattering spectroscopy (ISS) (Ref. 1) as well as related fields such as impact-collision ion scattering spectroscopy (ICISS), a special case of ISS where only ions scattered thru $\theta \approx 180°$ are considered,[2] secondary-ion-mass spectroscopy (SIMS) (Ref. 3) and direct-recoil spectroscopy (DRS) (Ref. 4) have been very effective in surface atomic-structure analysis and composition. In ISS, ICISS, and SIMS the scattered particles are typically energy and/or mass analyzed to derive useful information. Time-of-flight (TOF) techniques, used in DRS, offer a distinct advantage over the typical energy and mass analysis in that this method allows the detection of all scattered particles at once. These tools have also proved to be very powerful in probing the electronic properties of the surface. In the case where the ion is multicharged, as the ion with its large potential energy approaches the surface, scatters, and then recedes from it, neutralization processes will occur which give information directly relating to the electronic properties of the surface. Analysis proceeds thru the detection of electrons emitted during the scattering process and detection of the scattered particle's charge state, along with the distribution of any scattered excited atomic or ionic states. One specific measure of the interaction between the incident projectile's electronic state and the surface's electronic properties is the scattered charge fraction $R(r_j) = A^{r_j}/\sum_i A^{r_i}$, where r_i (r_j) are the scattered remnant charge states of the projectile A. This aspect of the multicharged ion-surface interaction is the subject of this paper. A review of recent developments in the applications of ion scattering spectroscopy such as surface reconstruction and the correspondence between the scattered ion fraction and the work function of the scattering surface has been given by Taglauer *et al.*[5]

A laser-operated ion source (LOIS) (Ref. 6) makes use of a high-power pulsed laser to focus the light onto a solid target with energies $\sim 10^{12}$ W/cm^2. This energy density is sufficient to produce a plasma with various charge states and inherent energies of a few keV, the correct energy range for ISS experiments. The laser ion source cannot compete with ion sources such as the electron-cyclotron resonance ion source (ECR) or the electron-beam ion source (EBIS) in terms of either the charge states produced or the ion current obtained.[7] Yet, this ion source does have the distinct advantage of producing low-energy ions without the necessity of any further processing such as may be needed to slow down ions extracted by a fairly high potential ~10 kV for both the ECR and EBIS sources.

One last noteworthy comment about the LOIS ion source relates to the possible surface damage resulting from the impinging ions. Electron spectroscopy techniques such as x-ray photoelectric spectroscopy (XPS), ultraviolet photoelectron spectroscopy (UVS), Auger electron spectroscopy (AES), and low-energy electron diffraction (LEED) have been widely accepted for years as surface analysis techniques. One reason for their popularity is that these techniques cause little or no damage to the surface being studied, unlike techniques involving massive projectiles which typically carry significant mo-

menta into the interaction with the surface resulting in a propensity for surface damage such as sputtering and, in the case of crystals, site defects. However, these electron spectroscopy techniques cannot approach the surface sensitivity of ISS, etc. LOIS produces ion doses incident on the surface for a given charge state (z) approximately ~ 100 ions/cm^2 per laser shot, or equivalently $\sim 0.03z$ nA/cm^2. Using an argument given by Rabalais,[4] a scattering surface with $\sim 10^{15}$ atoms/cm^2 would require approximately 60 days of continuous bombardment by $z=3$ ions to sputter a monolayer of the scattering surface, assuming a sputtering coefficient of unity. LOIS does not even approach this time scale for scattering surface exposure to the impinging ions, and hence the surface damage induced ought to be minimal.

APPARATUS

The apparatus is shown in Fig. 1 and has been described in greater detail elsewhere.[8] LOIS uses a Q-switched neodymium-doped yttrium aluminum garnet (Nd:YAG) laser to produce pulses ≈ 15 ns full width at half maximum (FWHM) with an energy ≈ 850 mJ. This laser beam (LB) is focused by some optics (OP) onto a solid laser target (LT) mounted inside the vacuum system. The solid cylindrical laser target, composed of individual C, Al, and Pb target disks, is continually rotated to provide a fresh surface for each laser shot, and is translated vertically to change target disks. A plasma plume (PP) consisting of multicharged ions in addition to the plasma electrons is created by the incident laser pulse. The plasma plume expands down the axis of the vacuum system toward a pair of plasma apertures (PA) restricting the unused portion of the plume to this section of the vacuum system. The collimated portion of the plasma plume then passes thru a plasma electron stripping screen. The ions proceed into a 180° cylindrical electrostatic analyzer (EA) which energetically selects the ions in the form of an energy-to-charge ratio (eV/z). This arrangement is, therefore, inherently suitable for the TOF technique which is employed with this apparatus. The signal strength of the multicharged ion packets exiting from the electrostatic analyzer is increased by a pair of identical Einzel lenses (EL). A particular ion packet, charge state, may be selected by an ion gate (IG) located between the two lenses. This feature proves very helpful in the analysis of complicated spectra where the charge state responsible for a given signal peak is unclear.

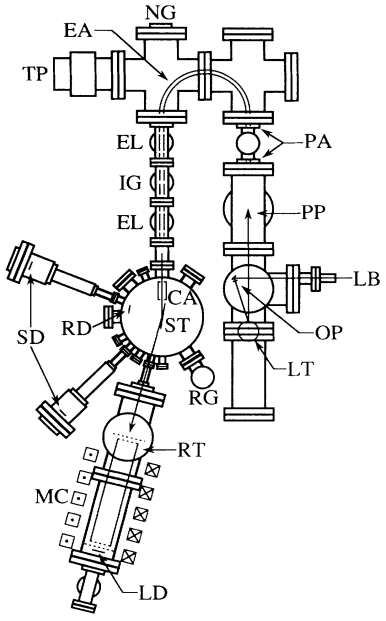

FIG. 1. Schematic diagram of vacuum system shown for long-arm CEMA detector (LD) at a scattering angle of 15° and short-arm CEMA detectors (SD) at 45° and 112.5°. Individual components also denoted in the diagram are laser beam (LB), optics (OP), laser target (LT), plasma plume (PP), plasma apertures (PA), electrostatic analyzer (EA), nude ion gauge (NG), turbomolecular pump (TP), Einzel lens (EL), ion gate (IG), circular apertures (CA), rotatable CEMA detector (RD), scattering target (ST), residual gas analyzer (RG), retarding tube (RT), and magnetic coils (MC).

The manipulated ion packet(s) enters the scattering chamber housing the scattering target (ST), presently a gold-plated first-surface optical mirror, which may be rotated while under vacuum. The center of the scattering target is located 193.2 cm from the laser target. The ion packet(s) is collimated immediately prior to interacting with the scattering target by a pair of circular apertures (CA). The important angles of this interaction of the incident projectile with the scattering surface are depicted in Fig. 2. The signal produced by the ion impact with the gold surface is detected with the use of a Galileo chevron channel-electron-multiplier array (CEMA). Several detectors are shown in Fig. 1 mounted on the scattering chamber ports. Two short-arm CEMA detectors (SD) are depicted at 45° and 112.5° scattering-angle port positions, as well as a long-arm CEMA detector (LD) at 15° located at distances of 44.2 and 76.4 cm from the center of the scattering target, respectively. Inside the chamber, 9.6 cm from the scattering target center, is a rotatable CEMA detector (RD). This detector may be continuously rotated from 0° to 135° scattering angle while under vacuum.

The long arm contains a retarding tube (RT) consisting of an electrically isolated stainless steel tube enclosed by stainless steel screens on both ends and mounted between

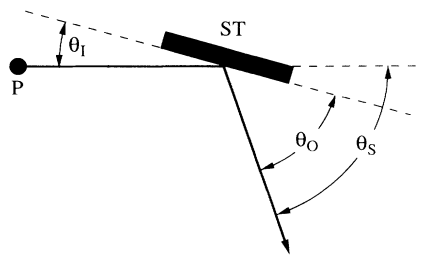

FIG. 2. Diagram illustrating the various angles concerned with the incident projectile (P) defined with respect to the scattering target's (ST) surface. The angles are incoming angle (θ_I), outgoing angle (θ_O), and scattering angle (θ_S).

two additional screens which are grounded. This feature allows the remnant charge of the scattered incident multicharged ions to be determined by the application of a positive potential to the tube, V_T. The ions are first decelerated in the gap produced by the first grounded screen and the front screen of the tube. The ions then drift in the equipotential environment of the retarding tube before being accelerated to their original energy while passing through the gap composed of the back screen of the tube and the second grounded screen. Hence, neutral atoms arrive at the long-arm CEMA detector first while the ion of the highest remnant charge state is detected latest in time. The CEMA detectors are operated with the front end of the detector at ground. Thus, all remnant charge states of the same incident ion packet strike the detector with the same velocity. Since the only remnant charge state observed in this study was Al^+ (see next section), having an ionization potential energy of 6.0 eV, small compared with kinetic energies ~ 1 keV, it is assumed that the signal produced by the CEMA detector due to a neutral Al atom is essentially the same as that produced by a singly charged Al ion. Magnetic coils (MC) mounted on the long arm produce a strong longitudinal magnetic field in the ion drift region of the retarding tube to prevent ion loss due to space-charge repulsion effects.

The turbomolecular-pump-based (TP) vacuum used in this study is an UHV system with a base pressure, remaining constant during data acquisition, $\approx 1.5\times 10^{-10}$ Torr in the scattering chamber. The pressure is monitored in this section of the vacuum system by a residual gas analyzer (RG) which detects only masses 2 and 28 amu (10^{-10}-Torr scale) when the entire vacuum system, excluding the turbo pumps, has been baked for several days at 200 °C. During the baking process the scattering target is individually heated by the tungsten screen filament which is the last item of the oven to be shut down in an effort to minimize the contaminants readsorbing onto the gold scattering surface as the system cools. A nude gauge (NG) located near the electrostatic analyzer measures a base pressure in this section of the vacuum system of $\approx 2\times 10^{-9}$ Torr and rising to $\sim 7\times 10^{-8}$ Torr during data acquisition. An argon discharge of the gold mirror is performed after the bakeout as the last step in the cleaning procedure of the scattering target. This is accomplished by the application of a potential ~ 1 keV to the electrically isolated gold mirror for a period of 30 s to a few minutes. The rotatable detector and a detector mounted on the 45° scattering-angle port are used to monitor the condition of the scattering target surface (described in more detail in the next section) after completion of the discharge. Further cleaning of the gold surface may be continued as necessary.

RESULTS

The scattering target prior to being subjected to the cleaning procedure (extended bakeout at 200 °C and an Ar discharge of the scattering target surface) and under a pressure $\sim 2\times 10^{-8}$ Torr appears to be contaminated mainly by atomic hydrogen and carbon. The signal obtained from incident C^{z+} ($z=1-4$) specularly reflected through 45° before and after cleaning as seen by the rotatable detector is shown in Fig. 3 (all spectra presented in this paper have a negative-going signal). The spectrum in Fig. 3(a) also indicates the FWHM time for elastic single scattering (SS) of C from C and elastic directly recoiled (DR) H from the incident C.[4] A negative potential of -200 V has been applied here to a screen located inside the detector housing. This potential serves to simplify the spectrum by rejecting the Auger electron signal produced when the ions strike the gold surface. A spectrum resulting from a clean "smooth" surface is given in Fig. 3(b). In this case, no electron-retarding potential has been applied and hence the appearance of Auger electron peaks (zE) preceding the scattered C peaks (zA). The corresponding Auger electron signal for incident C^+ ($1E$) is not detected. The energy of Auger electrons resulting from incident C^+ is ~ 1 eV maximum,[9] which is beyond the capabilities of the apparatus as no attempt has been made to magnetically shield the chamber. The scattered C spectra resulting after cleaning have times that agree well with those expected due to an elastic single-scattering event with the gold surface. Although the resolution of this detector is not good considering its close proximity to the scattering surface, other spectra obtained also indicate that H and C are the main surface contaminants. Carbon contamination of a gold surface has been reported elsewhere.[10]

Prior to any cleaning of the scattering surface no signal is seen by either the short-arm or the long-arm CEMA detectors. After baking the vacuum system, a weak and very wide signal is detected from the clean "rough" gold surface. This signal is illustrated for incident C^{z+} ($z=1-4$) in the solid spectrum in Fig. 4(a). The dashed

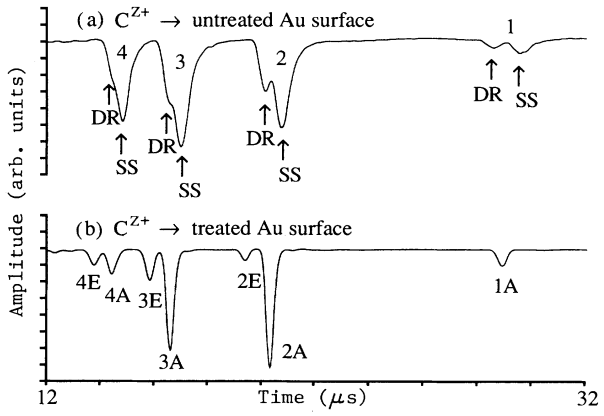

FIG. 3. TOF spectrum for ~ 280-eV/z incident C^{z+} ($z=1-4$) as seen by the rotatable CEMA detector at 45° specular reflection. Data taken (a) before performing an argon discharge of the scattering target's surface (untreated), and (b) after performing a discharge (treated). Elastic direct-recoil (DR) times for desorbed surface hydrogen from the incident carbon projectile, and elastic single-scattering (SS) times for the incident carbon projectile from surface-adsorbed carbon are indicated in (a). Scattered carbon peaks (zA) and their preceding Auger electron peaks (zE) corresponding to each projectile incident charge state (z) are denoted in (b).

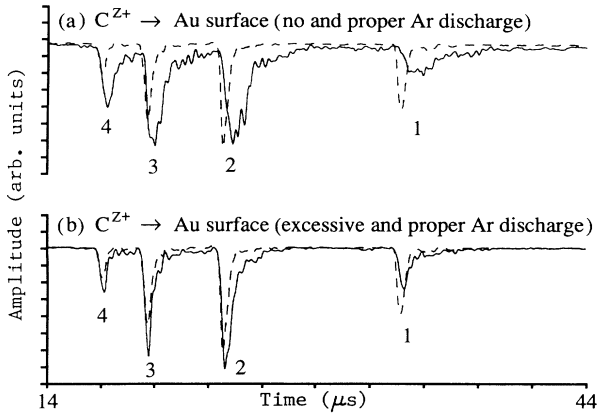

FIG. 4. TOF spectrum for ~280-eV/z incident C^{z+} ($z=1-4$) as seen by the rotatable CEMA detector at ≈45° specular reflection. Dashed line in both (a) and (b) represents typical signal seen after performing a proper discharge of the scattering target's surface. Typical signal seen with no discharge and an excessive discharge are illustrated in (a) and (b), respectively, by the solid lines.

spectrum in Fig. 4 is that obtained after performing a proper Ar discharge which has a smoothing effect on the scattering surface. The rotatable detector shows no detectable H or C contamination of the surface remaining after the discharge. The solid spectrum in Fig. 4(b) shows the signal resulting from an excessive discharge of the surface which is beginning to roughen the surface once again. This can be seen in the widening of the signal which is indicative of a bulk interaction between the carbon projectiles and the gold scattering surface. The smoothness of the scattering surface greatly affects both the magnitude and the remnant charge content of the scattered incident Al ions as shown in Fig. 5. This effect was noted in an earlier publication by Hughes *et al.*[11]

Three ion species were considered in this study, namely, C, Al, and Pb. For all cases considered, $\theta_S=15°$, 30°, and 45° specular reflection, C^{z+} ($z=1-4$) appeared to be completely neutralized ($r=0$ only) after being scattered from the gold surface, i.e., no detectable remnant non-neutral charge state ($r>0$) was ever observed. Due to a weak signal, Pb^{z+} ($z=2-6$) was investigated only for $\theta_S=15°$. Lead was also found to be completely neutralized ($r=0$ only) after interacting with the metal surface. A sample spectrum for Pb is given in Fig. 6 which also depicts the expected arrival times for the remnant singly charged state (z^{r+}, $z=3-6$, $r=1$).

The behavior of Al was markedly different as the remnant singly charged state was observed for all three cases, as shown in Fig. 7. Signal strength was too weak for accurate charge-fraction determination for the $\theta_S=30°$ and 45° cases. The charge fraction for the remnant singly charged state ($r=1$), $R=[Al^+]/([Al^+]+[Al^0])$, for both of these scattering angles is ~60–70 %. Figure 5(b) shows typical data from which the charge fraction is determined by the calculation of the respective signal areas. A search for higher remnant charge states ($r>1$) was conducted; however, none were detected. An example of this is given in Fig. 8, which shows the expected detection times for the remnant doubly charged state for the incident Al^{z+} (z^{r+}, $z=3$ and 4, $r=2$).

A more detailed study of the scattered charge component was performed for the 15° scattering angle. The incoming angle (for the outgoing angle, refer to Fig. 2) was varied from $\theta_I=3°-12°$ ($\theta_O=12°-3°$) while the scattered angle remained fixed at $\theta_S=15°$. Data were acquired for incident Al^{z+} ($z=3-5$) and $\theta_I=3.0°$, 5.0°, 7.5°, 10.0°, and 12.0°. The experiment was repeated three times using 1000 laser shots each for a given charge state and a given angle. The experimental curves found for each of the three incident charge states are depicted in Fig. 9 along with data points representing the average of

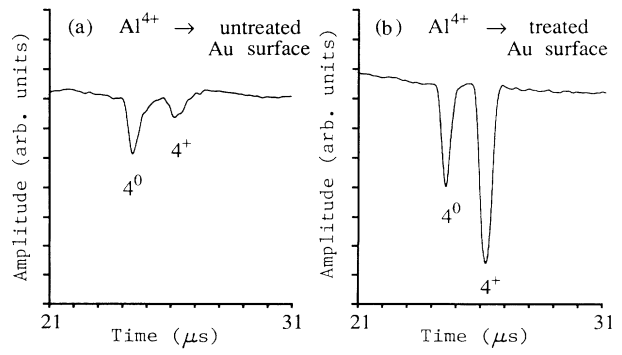

FIG. 5. TOF spectrum for ~1600-eV gated incident Al^{4+} as seen by the long-arm CEMA detector at 15° specular reflection. A positive potential has been applied to the retarding tube ($V_T=+960$ V.D.C.). Spectrum represents typical data obtained (a) before performing an argon discharge of the scattering target's surface (untreated), and (b) after performing a discharge (treated).

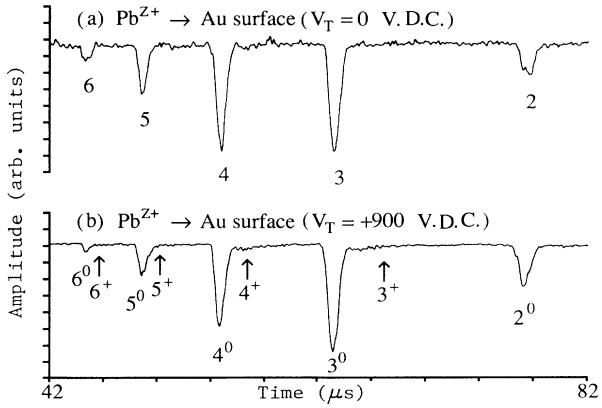

FIG. 6. TOF spectrum for ~620-eV/z incident Pb^{z+} ($z=2-6$) as seen by the long-arm CEMA detector at 15° specular reflection. Spectrum represents typical data obtained (a) with the retarding-tube potential (V_T) held near ground, and (b) with an applied positive retarding-tube potential. Peaks corresponding to the scattered neutral ($r=0$) and the expected arrival times for the remnant singly charged state ($r=1$) associated with each projectile incident-charge state (z) are denoted as z^{r+} in (b).

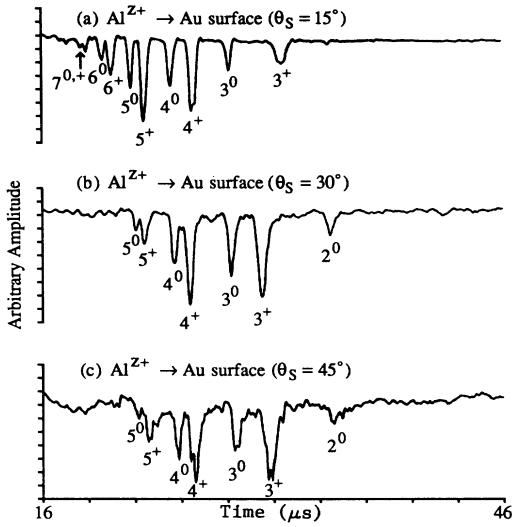

FIG. 7. TOF spectrum for ~400-eV/z incident Al^{z+} as seen by the long-arm CEMA detector at (a) 15° specular reflection ($z=3-7$) ($V_T=+900$ V.D.C.), (b) 30° specular reflection ($z=2-5$) ($V_T=+720$ V.D.C.), and (c) 45° specular reflection ($z=2-5$) ($V_T=+720$ V.D.C.). Peaks corresponding to scattered remnant charge states ($r=0$ and 1) associated with each projectile incident-charge state (z) are denoted as z^{r+}. The positive retarding-tube potential applied (V_T) in each case is given here.

the three runs for each of the five angles investigated.

Hagstrum's description of the probability $P(S,v_{I\perp},v_{O\perp})$ that an ion scattered from a metal surface (low-energy range) with known incoming normal velocity ($v_{I\perp}$) and outgoing normal velocity ($v_{O\perp}$) will be found in it's original charge state at a distance S from the metal surface ($S=0$ at plane of nuclei of surface atoms, Hagstrum[12]) can be changed to a charge fraction (R) for the case of a singly charged ion as

$$R=\exp\left[-v_c\left[\frac{1}{v_{I\perp}}+\frac{1}{v_{O\perp}}\right]\right], \quad (1)$$

with the characteristic velocity given by $v_c=A/a$ where A is usually interpreted to be the neutralization transition rate at the "scattering surface" ($S=0$) and a is the operative range of the neutralization process. Here, the remnant charge fraction includes contributions from both the incoming and outgoing paths of the incident ion's trajectory. The experimentally obtained curves for each of the incident charge states ($z=3-5$) considered independently (constant energy, $E\approx z\times 400$ eV) as displayed in Fig. 9 clearly shows that the observed charge fractions depend on the outgoing path, but not the incoming. Furthermore, all memory of the original multicharged-state nature of the incident ion ($z>1$) appears to be lost prior to the outgoing path of the projectile's trajectory, as only the remnant singly charged and neutral states of aluminum are detected after scattering regardless of the incident charge state. These observations are in line with the concept of a step-wise neutralization of the mul-

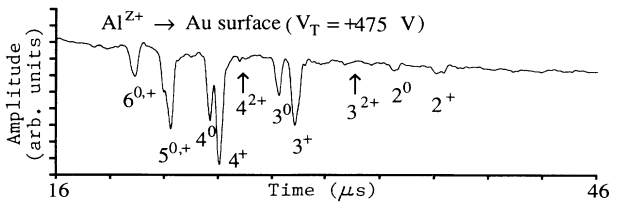

FIG. 8. TOF spectrum for ~400-eV/z incident Al^{z+} ($z=2-6$) as seen by the long-arm CEMA detector at 30° specular reflection. Peaks corresponding to the scattered remnant charge states ($r=0$ and 1) and the expected arrival times for the remnant doubly charged state ($r=2$) associated with each projectile incident-charge state (z) are denoted as z^{r+}. The positive retarding-tube potential applied (V_T) is given in the figure.

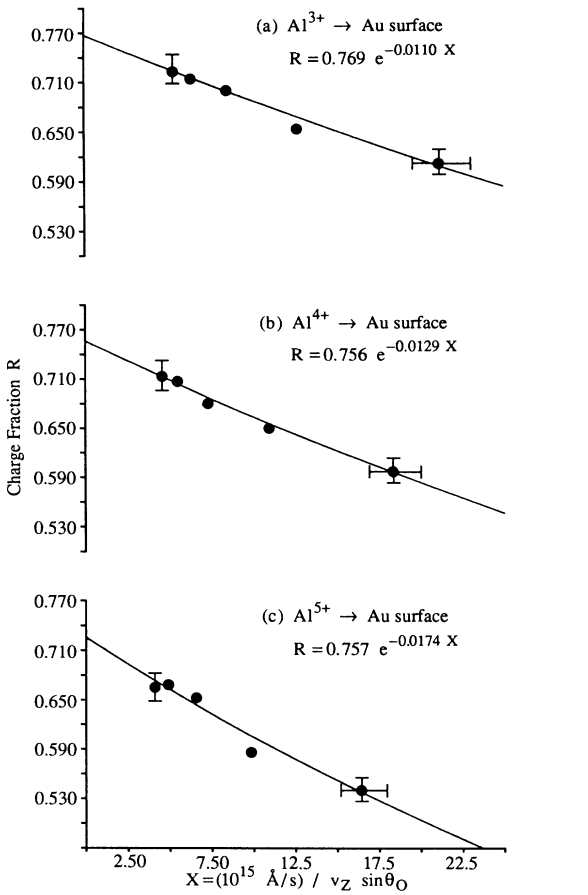

FIG. 9. Charge fraction, $R=[Al^+]/([Al^0]+[Al^+])$, for the scattered remnant singly charged and neutral states ($r=0$ and 1) resulting from ~400-eV/z incident Al^{z+} scattered thru 15° where (a) $z=3$, (b) $z=4$, and (c) $z=5$. Charge fraction is plotted as a function of the scattered normal (with respect to the scattering surface) projectile velocity ($v_Z\sin\theta_O$, $\theta_O=0°$ parallel to the scattering surface; see Fig. 2). Data points are plotted along with a few typical error bars representing the corresponding uncertainties $\Delta\theta=\pm 0.25°$ and $\Delta R=\pm 2.5\%$. Note the error bars corresponding to $\Delta\theta$ for the left data points ($\theta_O=12°$) are narrower than the data points and are therefore not shown. The solid curve, equation given in the figure, represents the result of an exponential weighted least-squares fit of the data.

ticharged ion during the incoming path.[13] The normal velocities of incident Al^{z+} ($z=3-5$, $E\approx 400$ eV/z) ranges from $v_{O\perp}\approx 5.0\times 10^{13}$ Å/s for Al^{3+} with $\theta_O=3.0°$ to $v_{O\perp}\approx 2.5\times 10^{14}$ Å/s for Al^{5+} with $\theta_0=12.0$. This may be compared to typical nonradiative neutralization processes with transition rates $\sim 10^{-15}$ s and neutralization distances ~ 5 Å/z [estimated distance using a 5.1-eV work function for Au (Ref. 14)]. Although these time and distance scales are only estimates, it seems reasonable that the velocities are slow enough that a picture of the incoming ion being neutralized in successive steps is a reasonable one. Higher remnant charge states have been observed for higher incident ionic charge states with greater normal velocities.[15] It should be noted that in recent years this step-wise neutralization model as proposed by Arifov has come under considerable scrutiny. In many cases the time needed for the neutralization of a highly charged projectile carrying core holes into the interaction with the surface via this cascade process is far greater than the time the projectile actually spends near the surface where these neutralization mechanisms occur. van Emmichoven, Havener, and Meyer[16] have found this to be the case where 24 keV N^{z+} ($z=2,4,6$) was scattered from a Cu(100) surface. Here, in order to obtain reasonable agreement with the experimental results, Arifov's model of resonant neutralization followed by purely atomic Auger transitions had to be modified to include Auger deexcitation where one electron from the metal is captured directly into a low-lying state of the projectile ion and a second metal electron is emitted into the vacuum.

The independence of the detected charge fraction on the incoming path was also observed by Kumar, Chen, and Rabalais[17] who investigated the charge fraction of several singly charged noble gases scattered from a crystalline yttrium surface. They suggested that the ions are completely neutralized on the incoming path ($\theta_I=6.5°$) with the final charge state depending on the degree of reionization occurring during the violent collision with the scattering surface atom(s) and the subsequent Auger and resonant neutralization processes experienced by the projectile on the outgoing path ($\theta_O\geq 22°$). Thus, the revised charge fraction may be expressed as

$$R=P_I e^{-v_c/v_{O\perp}}, \tag{2}$$

where P_I represents the ionization probability of the projectile during the violent collision. The inclusion of the violent collision region (see, for example, Verhey, Poelsema, and Boers[18]), in addition to the incoming and outgoing paths of the particle's trajectory dealt with since the first definitive studies by Hagstrum[12,19] as incorporated by Kumar, Chen, and Rabalais is an attempt to include neutralization, ionization, and excitation of the projectile resulting from the formation of a quasidiatomic molecule by the projectile and a surface atom.

An attempt was made to obtain an experimental curve for all three incident charge states together similar to that derived for each of them separately. The resulting curve is depicted in Fig. 10(a). Upon inspection of the data points, a distinct pattern emerges where all the incident Al^{3+} data points lie above the curve, the Al^{4+} lie near it, and the Al^{5+} lie below. The significance is that although the incident Al^{3+} for a given outgoing angle spends more time near the surface ($E\approx 1200$ eV) than the Al^{5+} ($E\approx 2000$ eV), the incident Al^{3+} produces the greater charge fraction. This is opposite to what is expected from the simple exponential decay behavior with a constant characteristic velocity. If the "constant" characteristic velocity is allowed to have an energy dependence, i.e., $v_c\rightarrow v_c(E)\propto E^n$, then a much better fit is found as given in Fig. 10(b). The energy exponent n of the "energy-dependent" characteristic velocity derived from the weighted least-squares fit is fairly insensitive in the range of $n=1.12\pm 0.10$ in the sense that the sum of the errors increases slowly in this range by $\approx 10\%$.

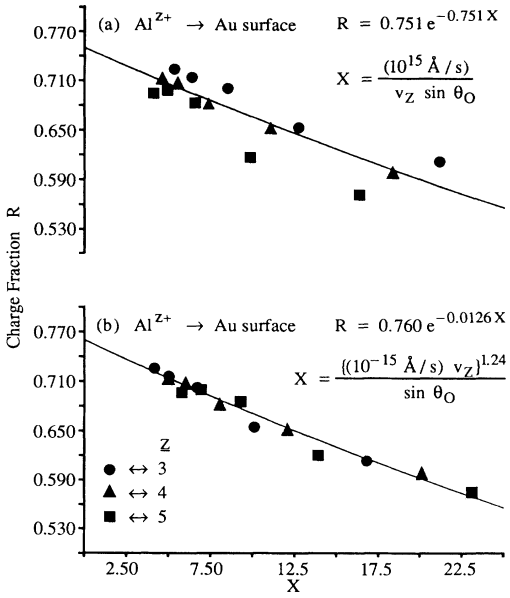

FIG. 10. Charge fraction, $R=[Al^+]/([Al^0]+[Al^+])$, for the scattered remnant singly charged and neutral states ($r=0$ and 1) resulting from ~ 400-eV/z incident Al^{z+} ($z=3$ to 5) scattered thru 15°. Charge fraction is plotted as a function of the scattered normal (with respect to the scattering surface) projectile velocity ($v_Z\sin\theta_0$, $\theta_0=0°$ parallel to the scattering surface; see Fig. 2), with (a) a constant characteristic velocity, and (b) an energy-dependent characteristic velocity. The solid curve, equation given in the figure, represents the result of an exponential weighted least-squares fit to the data.

An energy dependency of the characteristic velocity has been observed by others. This effect was seen by Garrett, MacDonald, and O'Connor[20] for Al^+ sputtered from an aluminum target by incident Ar^+. A more detailed study of this energy dependency was performed by MacDonald and O'Connor[21] where incident He^+ and Ne^+ with an energy range of 0.1–3.0 keV were scattered thru 90°. A detector was used which could be moved in a plane perpendicular to the plane containing the incoming ion and the surface normal vectors. This allowed the scattering angle of the ions to remain constant at 90° while varying the outgoing angle with respect to the surface. MacDonald and O'Connor were thus able to inves-

tigate the outgoing-path contribution to the neutralization of the scattered particle since the normal velocity of the projectile varies with this orientation angle while the same scattered velocity is maintained (constant scattered energy and, therefore, any charge change occurring in a violent collision region should be roughly constant). For a given incident ion energy, the charge fraction determined for the data points representing the different surface orientation angles could be fit to an exponential decay with a constant characteristic velocity. However, as the projectile's incident energy was varied, the characteristic velocity showed a scattered-energy dependence (velocity on the outgoing path).

A simple theoretical description has been proposed by Akazawa and Murata[22] to explain the energy dependence of the characteristic velocity which they have also observed.[23] It is pointed out that Hagstrum's original theory[12] includes an energy dependence as seen in the transition rate for a given charge-change mechanism.

$$R_t(S=S_0)=Ae^{-aS_0} \tag{3}$$

where S_0 is the distance of closest approach, an energy-dependent parameter. This leads to the following form for the charge fraction with $P(S,v_{O\perp})$ normalized such that $P(S_0,v_{O\perp})=1$ (Ref. 24)

$$R=\exp\left[-\frac{A}{a}\left[\frac{1}{v_{I\perp}}+\frac{1}{v_{O\perp}}\right]e^{-aS_0}\right], \tag{4}$$

so

$$v_c=\frac{A}{a}\rightarrow v_c=\frac{A}{a}e^{-aS_0}. \tag{5}$$

A charge fraction sensitive to the distance of closest approach would aid in the explanation of the disappearing charge content of the incident aluminum for a rough surface where the ion-surface interaction is more intimate, i.e., smaller S_0 (refer to Figs. 4 and 5, and Hughes *et al.*[11]). This can be understood in terms of the shadow cones of neighboring gold atoms of a rough surface no longer aligning in such a manner as to prevent scattering processes resulting from small-impact parameters. Akazawa and Murata assume the ion-surface interaction may be expressed as

$$V(S)=Be^{-bS}, \tag{6}$$

where B and b are suitable constants. Then, for simplicity, they assume that the parallel component of the velocity is nearly conserved in specular reflection and proceed to equate the perpendicular energy of the projectile to $V(S)$ with the final result being

$$R=\exp\left\{-\left[\frac{A}{av_\perp}\left[\frac{m}{2B}\right]^{a/b}v_\perp^{2a/b}\right]\right\} \tag{7}$$

or

$$v_c\propto v_\perp^{2a/b}, \tag{8}$$

where m is the mass of the projectile. Since the repulsive potential and the neutralization processes both depend on the overlap of the same wave functions in the low-energy region, $a\approx b$ should be a reasonable approximation and, therefore, $v_c\propto v_\perp^2$. It can be calculated that Al^+ specularly reflected through 15° with $E\approx1600$ eV has $S_0\approx1.2$ Å (Ref. 25). Considering, for simplicity, crystalline gold with a lattice spacing of ≈4.0 Å, it is also found that the aluminum projectile is essentially scattered by one specific surface gold atom, "quasi"-single-scattering, for all θ_I (θ_O) considered in this investigation where $\theta_S=15°$. The same argument can be applied to incident Al^+ with $E=1200$ and 2000 eV, which correspond to incident Al^{3+} and Al^{5+}, respectively. Consider a specific outgoing angle, for example choose $\theta_O=7.5°$. This would give

$$v_c\propto v_{O\perp}^2=v_O^2\sin^2 7.5°\propto v_O^2\propto E,$$

where only the outgoing-path contribution to v_c has been included and E is the initial projectile energy. An energy dependence for the characteristic velocity as just described agrees well with the results obtained as portrayed in Fig. 10(b).

The relationship of the Fermi level (F) of the metal and the ionization level (E_i) of the projectile plays a very important role in the charge fraction observed. Figure 11 is a schematic diagram of the energy levels, measured relative to the vacuum level, pertinent to the outgoing pass. The ground levels are shifted up due to the image potential as

$$E_i(S)=E_i(\infty)-(3.6\text{eV})/S, \tag{9}$$

where S is measured in Å. It is evident from this diagram that the carbon ground state, $E_i(\infty)=11.3$ eV, is in resonance with the valence band from $S\approx0.6$ Å (assuming for the moment that this simple form for the image potential holds in this region) where $E_i(0.6)\approx F=5.1$ eV to $S\approx5.1$ Å where $E_i(5.1)=10.6$ eV. Past this distance from the surface, the carbon ground state falls below the bottom of the valence band. Even if the carbon projectile were to start its outgoing path as a singly charged ion, it would be quickly neutralized as it moves away from the surface by resonance neutralization from the valence band. The ground state of lead, $E_i(\infty)=7.6$ eV, is in resonance with the valence band for $S\approx1.5$ Å to $S=\infty$.

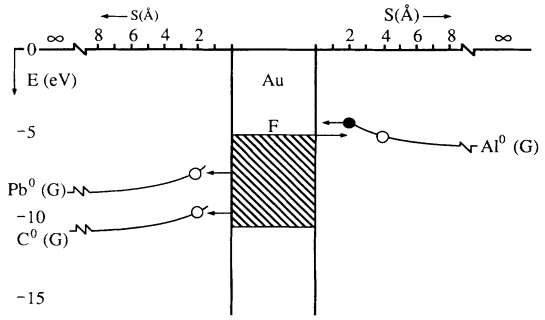

FIG. 11. Schematic-energy diagram illustrating the ground-state energy levels of neutral carbon, aluminum, and lead denoted as $C^0(G)$, etc., as a function of the distance (S in Å) from the gold scattering surface. Also depicted is the Fermi level (F) of the conduction band.

Again, as for carbon, lead would likewise be expected to be completely neutralized as it moves away from the scattering surface.

Aluminum scatters dominantly into the remnant singly charged state. The ground state of aluminum is in resonance with the Fermi level at $S \approx 4.0$ Å. This should be more accurate as S is larger. In this region Auger and certainly resonance neutralization processes should be very effective. If the ground state were to simply move above the Fermi level in this region, then one would expect to observe mostly singly charged ions due to resonance ionization of any aluminum projectiles in the region $S \leq 4.0$ Å. Any detected neutralized aluminum would then need to be created during the outgoing path with $S > 4.0$ Å. This offers a seemingly logical explanation for the charge fraction observed for a given scattered projectile energy, i.e., dependence on the outgoing path only. However, it fails when the observed energy dependence of the characteristic velocity is included. A greater neutralization is found for higher energies, which is inconsistent with the above as the ground-state energy level should remain above the Fermi level and hence any neutralization occurring close to the surface will be resonantly reionized.

The problem is twofold. How accurately an exponential decay describes the neutralization of the projectile in the region where S is small, less than an Å, is unclear. Additionally, the broadening of the ground state of the projectile as it interacts with the valence electrons has been thus far ignored. It is difficult here to make any definite conclusions involving the details of the ground-state behavior for aluminum in the region close to the gold surface as little is known at the present time. Calculations given by Brako and Newns[26] for Na^+ scattered from a metal surface show that the ground state can broaden approximately equal to a few eV close to the surface. The importance of this effect on the ground state to the neutralization processes particularly depends on the nature of the energetic overlap of this broadened state with that of the conduction band as the state evolves close to the surface where the overlap of the wave functions is already significant. One statement that can be made is that there must exist a mechanism in this region to break the symmetry of the incoming and outgoing paths, i.e., the charge fraction is only dependent on the latter. The two paths are already asymmetric in the sense that the incoming particle is a multicharged ion, yet this is not thought to play a significant role in the final charge state of the aluminum projectile, i.e., the multicharged ion is thought to be quickly neutralized to the singly charged state which then continues to approach the gold surface in the region of interest.

Lastly, it is difficult to arrive at a reasonable explanation for the multiplicative constant to the decaying exponential of 0.760 [refer to Fig. 10(b)]. Inclusion of the energy dependence of the characteristic velocity relating to the distance of closest approach to the surface would appear to exclude an argument for this constant via the violent collision region similar to that made by Kumar, Chen, and Rabalais. The reason is that they assumed reionization of the projectile to take place in the violent collision region resulting in a given charge fraction existing at the beginning of the outgoing path where Auger and resonant neutralization of the ions then occurred as the projectile progressed along its outgoing path. In this investigation, for a given outgoing angle the distance of closest approach changes with respect to the energetically variant projectile. Hence, it would seem reasonable to expect the charge fraction existing at the beginning of the outgoing path to depend on this distance of closest approach instead of being a constant as experimentally observed here (refer to Fig. 9).

SUMMARY

In summary, the charge fractions of the ion species studied in this velocity range have been found to depend on several parameters. If the first ionization level of the incident ion lies significantly below the Fermi level of the metal valence band (e.g., Al at 6.0 eV, $r=0$ and 1, and Pb at 7.6 eV, $r=0$ only, compared with $F=5.1$ eV for Au), the projectiles appear to scatter only into the neutral state at these velocities. The observed charge fraction for the remnant singly charged state depends on normal velocity on the outgoing path and not the incoming. All memory of the multicharged-state nature of the incident ion appears to be lost prior to the outgoing path of the projectile's trajectory. The inclusion of an energy-dependent characteristic velocity which incorporates the distance of closest approach to the surface by the projectile is found to be necessary in order to obtain agreement with the data. The higher neutralization of the aluminum projectile observed for a deeper penetration of the gold surface as the incident projectile's velocity increases is consistent with the disappearing charge content seen as the surface character becomes rougher. The observed independence of the incoming path on the scattered charge fraction of the incident aluminum ions as well as the preceding multiplicative coefficient to the decaying exponential cannot be explained at this time. A satisfactory explanation will likely require a more detailed knowledge of the evolution of the aluminum ground state as it nears the surface gold surface.

ACKNOWLEDGMENT

The research described here was supported by the National Science Foundation through Grant No. DMR-85-76109, jointly funded by the Atomic, Molecular, and Plasma Physics Program, and the Solid State Program.

*Present address: Department of Physics, University of Tennessee, Knoxville, TN 37919.

†Present address: Alabama School of Mathematics and Science, Department of Physics, Mobile, AL 36616-2628.

‡Present address: Department of Physics, Peking University, Beijing 100871, People's Republic of China.

[1]D. P. Smith, J. Appl. Phys. **38**, 340 (1967).

[2]M. Aono, Nucl. Instrum. Methods B **2**, 374 (1984).

[3]A. Benninghoven, Appl. Phys. **1**, 3 (1973).
[4]J. W. Rabalais, CRC Crit. Rev. Solid State Mater. Sci. **14**, 319 (1988).
[5]E. Taglauer, M. Beckschulte, R. Margraf, and D. Mehl, Nucl. Instrum. Methods B **35**, 404 (1988).
[6]R. H. Hughes, R. J. Anderson, C. K. Manda, M. R. Carruth, L. G. Gray, and J. P. Rosenfeld, J. Appl. Phys. **51**, 4088 (1980).
[7]I. G. Brown, *The Physics and Technology of Ion Sources* (Wiley, New York, 1989).
[8]R. D. Miller, Ph.D. dissertation, University of Arkansas, 1990.
[9]R. H. Hughes, G. Wattuhewa, R. D. Miller, X. M. Ye., and D. O. Pederson, Phys. Rev. B **36**, 9003 (1987).
[10]F. W. Meyer, C. C. Havener, S. H. Overbury, K. J. Snowdon, D. M. Zehner, W. Heiland, and H. Hemme, Nucl. Instrum. Methods B **23**, 234 (1987).
[11]R. H. Hughes, R. D. Miller, G. Wattuhewa, X. M. Ye., and D. O. Pederson, Phys. Rev. B **40**, 43 (1989).
[12]H. D. Hagstrum, Phys. Rev. **96**, 336 (1954).
[13]U. A. Arifov, L. M. Kishinevskii, E. S. Mukhamadiev, and E. S. Parilis, Zh. Tekh. Fiz. **43**, 181 (1973) [Sov. Phys. Tech. Phys. **18**, 118 (1973)].
[14]P. Apell, Nucl. Instrum. Methods B **23**, 242 (1987).
[15]S. T. de Zwart, T. Fried, U. Jellen, A. L. Boers, and A. G. Drentje, J. Phys. B **18**, L623 (1985).
[16]P. A. Zeijlmans van Emmichoven, C. C. Havener, and F. W. Meyer, Phys. Rev. **43**, 1405 (1991).
[17]R. Kumar, Jie-Nan Chen, and J. W. Rabalais, Langmuir **1**, 294 (1985).
[18]L. K. Verhey, B. Poelsema, and A. L. Boers, Nucl. Instrum. Methods **132**, 565 (1976).
[19]H. D. Hagstrum, Phys. Rev. **96**, 325 (1954).
[20]R. F. Garret, R. J. MacDonald, and D. J. O'Connor, Surf. Sci. **138**, 432 (1984).
[21]R. J. MacDonald and D. J. O'Connor, Surf. Sci. **124**, 423 (1983).
[22]H. Akazawa and Y. Murata, Phys. Rev. B **39**, 3449 (1989).
[23]H. Akazawa and Y. Murata, Phys. Rev. Lett. **61**, 1218 (1988).
[24]H. D. Hagstrum, in *Inelastic Ion-surface Collisions,* edited by John C. Tully and C. W. White (Academic, New York, 1977).
[25]O. S. Oen, Surf. Sci. **131**, L407 (1983).
[26]R. Brako, and D. M. Newns, Surf. Sci. **108**, 253 (1981).